Gated SPECT with Technetium-99m-Sestamibi for Assessment of Myocardial Perfusion Abnormalities

F. Mannting and M.G. Morgan-Mannting

Nuclear Medicine Section, Department of Clinical Physiology, University Hospital, Uppsala, Sweden

High counting statistics with ^{99m}Tc-sestamibi make gated SPECT imaging realistic. Information obtained with gated and nongated SPECT were compared in 83 subjects (20 normals, 63 patients) using a 1-day protocol (250 MBq [6 mCi] rest, 900 MBq [24 mCi] peak stress). Studies were acquired for eight frames/RR interval and formatted to a standard nongated study, a study consisting of diastolic (DIA) frames and dynamic functional studies. The right ventricle appeared more distinct in DIA than in nongated studies ($p < 0.01$). The left ventricular cavity was larger in DIA studies ($p < 0.001$), leading to more coronal slices with cavity ($p < 0.001$). A strong inverse relation between left ventricular cavity size in nongated studies and increase in cavity size and in number of coronal slices with cavity in DIA studies was found ($r = -0.74$ and -0.67, both $p < 0.001$). Severity (extent and degree) of perfusion abnormalities in rest and stress studies, assessed quantitatively in 50 patients (20 normals as reference), correlated highly in nongated and DIA studies ($r = 0.98$, $p < 0.001$). Severity of small and moderate sized perfusion defects showed a high degree of agreement in nongated and DIA studies, while severity of large defects was less pronounced in DIA studies ($p < 0.05$). In patients with subtle perfusion abnormalities, the results from DIA imaging agreed best with clinical data.

J Nucl Med 1993; 34:601–608

High photon energy leading to less scatter and less tissue attenuation and counting statistics high enough to make gated SPECT clinically realistic are favorable characteristics of the new ^{99m}Tc-based perfusion imaging agent 2-methoxy-isobutyl-isonitrile (sestamibi). In theory, gated imaging of myocardial perfusion should lead to better image resolution by reducing the blurring effect of cardiac motion. Hence, regional differences in radionuclide uptake (perfusion) could become more clearly distinguished, potentially allowing detection of smaller perfusion abnormalities. Moreover, diastolic images extracted from gated studies may eliminate the problem with the partial volume effect (*1*), i.e., the effect of variations in regional systolic wall thickening on observed regional tracer uptake (uptake differences not conditioned by differences in regional perfusion per se). Also, dynamic gated SPECT images may contain regional function information.

Gated planar perfusion studies with ^{201}Tl (*2–6*) and sestamibi (*7–10*) found clearer edge definition, detection of perfusion abnormalities with higher frequency and with higher level of confidence (*8*) and improved detection of reversibility (*6*). Additionally, regional function expressed as wall motion or systolic wall thickening was obtained (*7–10*). Gated SPECT imaging has been applied in only a few studies involving small patient groups using ^{201}Tl (*11*) or sestamibi (*12–16*). These studies found advantages of gated SPECT with respect to high contrast perfusion images and additional regional functional information expressed as regional wall motion (*11–14,16*) or systolic wall thickening (*11–13,15*). Processing the huge amount of data in gated SPECT was a problem. The present study systematically compares quantitatively assessed myocardial perfusion abnormalities with nongated versus gated SPECT technique and sestamibi.

The aim of this study was to: (1) evaluate the feasibility and benefit of gated SPECT with sestamibi, (2) specifically compare quantitatively assessed perfusion abnormalities in simultaneously obtained nongated and gated studies and (3) examine the potential usefulness of obtained functional information.

PATIENTS AND METHODS

Normal Database

Twenty subjects, 10 normal volunteers (approved by the University Ethics Committee) and 10 patients (free of coronary artery disease (CAD) as determined by coronary angiography) (11 males and 9 females, mean age 51.2 yr ± 8.1 yr, range 37–68), served as the reference population. A database of normal regional myocardial uptake was established by means of an earlier described quantification method (*17*). Briefly, mean uptake in predefined myocardial segments at basal, mid and apical

Received Apr. 20, 1992; revision accepted Nov. 17, 1992.

For correspondence or reprints, contact: Finn Mannting, MD, PhD, Dept. of Radiology/Nucl. Med. Div., Brigham and Women's Hospital, Harvard Medical School, 75 Francis St., Boston, MA 02115.

myocardial thirds were determined. Lower limits of normal uptake distribution, defined as mean uptake −2 s.d. were established for stress and rest studies for each segment and myocardial level. Normal databases were created for the following protocols: (1) nongated rest and stress MIBI for 1- or 2-day protocols and (2) gated sestamibi SPECT (diastolic) rest and stress studies.

Patients

Gated SPECT was attempted in 63 consecutive patients with sinus rhythm. Gated SPECT was possible in 61 patients. It could not be performed in two due to frequent premature beats. One patient was excluded due to extreme interfering intestinal sestamibi retention. Gated stress and rest studies were available in 50 patients, while in 10 patients only gated, stress SPECT studies were obtained due to technical/practical nonpatient related problems.

The 50 patients enrolled in the part of the study comparing perfusion abnormalities in nongated and DIA studies consisted of 31 males and 19 females, mean age 55.3 yr ± 12.3 yr (57.8 yr ± 9.3 yr and 51.2 yr ± 15.5 yr, respectively). All patients were referred for evaluation of signs or symptoms of CAD. All patients had documented myocardial infarction and/or recent (< 12 mo) coronary angiography.

Stress Testing

Upright bicycle stress testing was performed according to a standard protocol. The patients stopped cardiovascular medication 24 hr prior to examination. Baseline ECG, heart rate and BP were recorded before starting on the bicycle and every 2 min during exercise. Workload started at 20 W and increased by 20 W every 2 min. The tracer was injected at maximal tolerable chest pain, exertion or dyspnea, and exercise continued for an additional 90 sec.

Gated SPECT Imaging Protocol

All patients were investigated according to a one-day rest/stress protocol (*18*). Technetium-99m-sestamibi (6.8 mCi [250 MBq]) was injected at rest. The patients ingested a high fat-content meal 15 min postinjection. Rest SPECT imaging began 1 hr postinjection. A commercially available software program (Gated SPETS, Nuclear Diagnostics AB, Stockholm, Sweden) running in the TSX (= MSE) operating system controlled the gated SPECT acquisition. The patients were connected to an ECG monitor for continuous display and control of ECG quality and trigger function, and the camera was interfaced to a standard computer (PDP 11/73, Digital Equipment Corp., Maynard, MA). Gate tolerance was set to ±15% around a mean RR interval computed as average of the last 16 heart cycles prior to start of acquisition. Data were acquired over a 180° rotation, from LPO 45° to RAO 45°, 32 angles, 32 sec and 8 temporal frames/angle (Fig. 1), in a 64 × 64 matrix. All studies were acquired on the same gamma camera (SX 300, Picker Intl., Bedford, OH) using a low-energy, high-resolution, parallel, hexagonal hole collimator.

Immediately following the rest study, the patients were stressed according to the stress protocol described. At peak exercise, 24.3 mCi (900 MBq) ^{99m}Tc-sestamibi was injected. Fifteen minutes after completion of stress testing, the patients ingested a high fat-content snack. Stress imaging started 45–60 min postinjection using the same acquisition protocol as for the rest study.

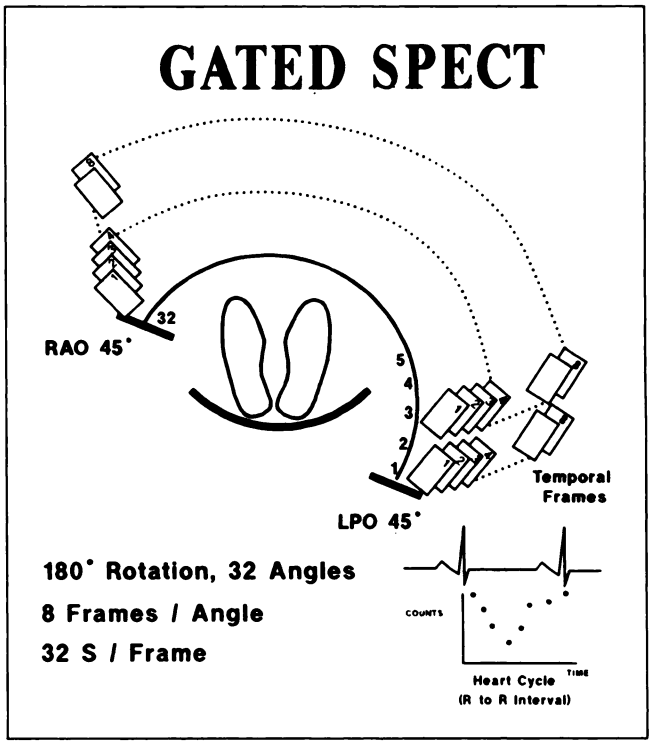

FIGURE 1. Schematic illustration of the gated SPECT acquisition principle and acquisition parameters. Note eight temporal frames per heart cycle (frames are used to describe parts of the heart cycle, i.e., in temporal context).

Filtering and Reconstruction

All acquisition studies were pre-filtered with a two-dimensional count-adaptive FFT Metz filter (*19*) using an array processor (AP 400, Analogic Corporation, Wakefield, MA). All gated sestamibi SPECT studies were reconstructed using eight temporal frames. Attenuation correction was performed after body outline definition (*20*). Software zoom (2x) was applied during the reconstruction. Reconstruction was performed by filtered backprojection (ramp filter) using commercially available software (GREK, Nuclear Diagnostics, Stockholm, Sweden). Standard transversal and true cardiac sagittal (long-axis) and coronal (short-axis) slices (6.1 mm) were created after individual determination of the heart axis.

Formatting

The acquired gated SPECT data may be formatted into various types of studies. For this investigation, the data from stress and rest studies were formatted into the following studies:

1. Traditional Nongated Study. The data acquired in each angle were summarized to a nongated conventional SPECT study.
2. Diastolic Studies (DIA). A study consisting of only diastolic frames, defined as frames with large constant left ventricular (LV) cavity size. A coronal slice at the midventricular level is selected and the corresponding eight temporal frames displayed. The frames with constant LV cavity were selected, guided by an adjustable, semi-automatic region of interest placed along the endocardium. The algorithm then automatically extracts the diastolic frames

from the remainder of the data and creates transversal/coronal/sagittal studies, consisting of the data representing the diastolic phase.

3. Dynamic Studies. Dynamic studies (cines) were created by adding spatial coronal slices to evenly divide the myocardium into three portions representing basal, mid and apical thirds. Also, a mid-sagittal, long-axis cine was created by selecting the mid-ventricular slice and adding one slice on either side.

Assessment of Perfusion Abnormalities

Quantification of perfusion abnormalities in the nongated and gated SPECT stress/rest studies was accomplished by a previously published method (*17*). Briefly, epicardial and endocardial borders were automatically defined. This definition may be manually adjusted to snugly fit the myocardium. The center of the left ventricular cavity was marked, and the myocardium (defined as the area between the epicardial and endocardial borders) was divided into segments. For the purposes of this investigation, 5° angle divisions were used.

Mean counts per segment for stress and rest were computed and displayed in a polar circumferential plot. Patient myocardial uptake distribution was compared to the normal database, segment by segment, at the various myocardial levels for each imaging protocol.

Abnormal segments were automatically identified (i.e., number of abnormal segments = extent of perfusion abnormality) if the patient distribution in any given segment fell below the lower normal limit for that particular myocardial portion and segment location.

Severity of perfusion defects (extent and degree) was computed by integrating the areas between the patient's activity distribution curves below the curve for the normal database distribution. The difference between stress and nonstress total scores represent the reversibility score.

Special adjustment for the one-day sestamibi protocol: In one-day rest/stress sestamibi studies, the majority of the rest uptake remained in the myocardium (*21,22*) and added to the assessed activity in the stress studies. Segmental rest uptake was therefore decay-corrected for elapsed time between imaging, giving remaining activity, and then subtracted (segment by segment) from the assessed stress activity, yielding true stress uptake. If no rest activity was present (as in separate-day rest/stress protocols), no such correction was required and this step of the program was skipped.

Reproducibility of the severity score assessment was shown to be high in a previous study (*17*) and not significantly affected by the adjustments used for the one-day sestamibi protocol.

Concordance analysis between overall results of quantified myocardial perfusion evaluation with nongated and DIA imaging technique was accomplished by categorizing the overall study results with each technique as: no abnormalities, ischemia or permanent abnormality.

Right Ventricular Uptake

The target-to-background (BKG) ratio for the right ventricle myocardium (RV) was calculated from corresponding mid-ventricular coronal slices in the nongated and DIA studies. A region of interest (ROI) was placed over the area of the RV myocardium containing the maximum counts. RV BKG activity was determined by placing a ROI 3–5 pixels lateral to the RV. Mean counts per pixel for the RV and BKG ROIs were recorded and peak RV/BKG ratio computed. A ROI was also placed over the area of LV myocardium with the highest uptake. Mean counts per pixel for LV myocardium was obtained, and a peak RV-to-peak LV uptake ratio computed.

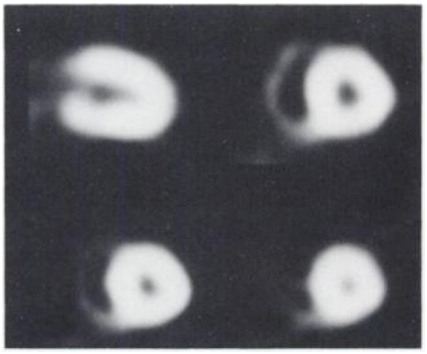

FIGURE 2. Simultaneous display of reconstructed dynamic (cine) studies. Mid-sagittal, basal-, mid-, and apical-coronal studies are created by adding slices and displayed as cines. Wall motions in all anatomical portions, including the apex, are evaluated and may be compared.

Left Ventricular Cavity Size

Corresponding mid-ventricular slices from the nongated and DIA studies were selected for determination of LV cavity size. Endocardium-to-endocardium distance (number of pixels, mean of two assessments) for the nongated and the DIA studies was assessed.

Number of Coronal Slices with Cavity

The number of useful coronal slices, defined as slices with LV cavity, for the nongated and DIA studies were determined. Nongated and DIA coronal studies were displayed separately on a high resolution color monitor using the same color table. The number of coronal slices with identifiable LV cavity were counted in each study.

Dynamic Studies

The mid-sagittal, basal, mid and apical coronal dynamic studies were displayed simultaneously (Fig. 2). Regional wall motion was assessed visually segment by segment, aided by an ROI marking ED edge displayed in overlay mode.

Statistical Methods

All values are given as mean ± s.d. unless otherwise indicated. Relationships between variables were analyzed by linear or nonlinear regression analysis and a p value < 0.05 was considered significant. Agreement between the methods was evaluated by the Bland-Altmann method (*22*). Comparisons between patients or groups were done with paired or unpaired t-tests. A p value of < 0.05 was considered significant.

RESULTS

Imaging times, processing times and secondary memory requirements for gated SPECT compared to standard SPECT are summarized in Table 1. Gated SPECT studies, when attempted, could be obtained in all but two patients (due to arrhythmia during acquisition). The success rate for obtaining gated SPECT in these consecutive patients was >96%.

TABLE 1
Summary of Acquisition and Processing Time, and Storage Requirement for Standard SPECT and Gated SPECT

	Std SPECT	G-SPECT	Incr
Acquisition time	20 min	30 min	50%
Filtering/Reconstruction	10 min	25 min	150%
Formatting	N/A	8 min	—
Total	30 min	63 min	110%
Storage requirements	1.5 MB	8.3 MB	550%

Std SPECT = standard SPECT, G-SPECT = gated SPECT, Incr = percent increase from Std SPECT to G-SPECT, and N/A = not applicable to standard SPECT studies.

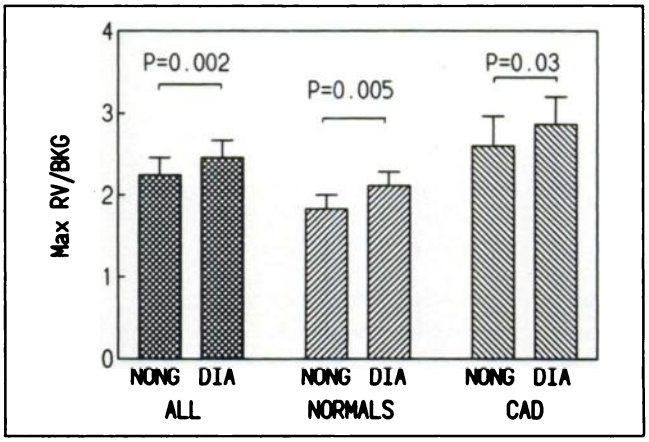

FIGURE 3. The maximal RV uptake-to-background ratio in nongated studies and DIA studies from the gated studies are shown for all subjects, normals and patients with CAD.

Right Ventricular Myocardial Uptake

Right ventricular wall motions were clearly visualized in the dynamic studies, and the right ventricle appeared more distinct in DIA studies than in nongated studies, an impression verified by a significantly higher RV-to-BKG ratio in DIA studies ($p < 0.01$) (Fig. 3). This was not an effect of lower BKG activity in the DIA studies, since peak RV-to-peak LV ratio also was significantly higher in the DIA studies than in the nongated studies (0.37 ± 0.09 versus 0.33 ± 0.11, $p < 0.01$), while the peak LV-to-BKG ratio was not significantly different in the nongated versus DIA studies (6.48 ± 1.52 versus 6.59 ± 1.62, $p = 0.46$, ns).

Left Ventricular Cavity Size

The LV cavity size assessed at corresponding mid-ventricular levels (Fig. 4A) was larger in DIA studies versus nongated studies (10.2 ± 3.8, 8.0 ± 4.0, $p < 0.001$) and in normals as well as in the patients (9.1 ± 2.3 versus 6.5 ± 1.9 and 12.5 ± 1.6 versus 10.4 ± 1.8, respectively, $p < 0.001$). The LV cavity extended further in the apical direction (Fig. 4A), leading to more coronal slices with ventricular cavity (14.0 ± 3.1 versus 12.1 ± 3.8, $p < 0.001$) and a decrease in the size of the "apex" (i.e., the portion of LV myocardium without cavity which is notoriously difficult to evaluate quantitatively in traditional nongated perfusion studies). A strong inverse, nonlinear relation between LV size in nongated studies and an increase in LV cavity size and number of coronal slices with ventricular cavity in the DIA studies were found ($r = -0.74$ and -0.67, respectively, $p < 0.001$, Fig. 5). This effect is particularly evident in patients with small hearts or hearts with small cavities.

Quantified Perfusion Abnormalities

Five patients showed no perfusion abnormality in rest or stress studies with neither nongated nor gated SPECT;

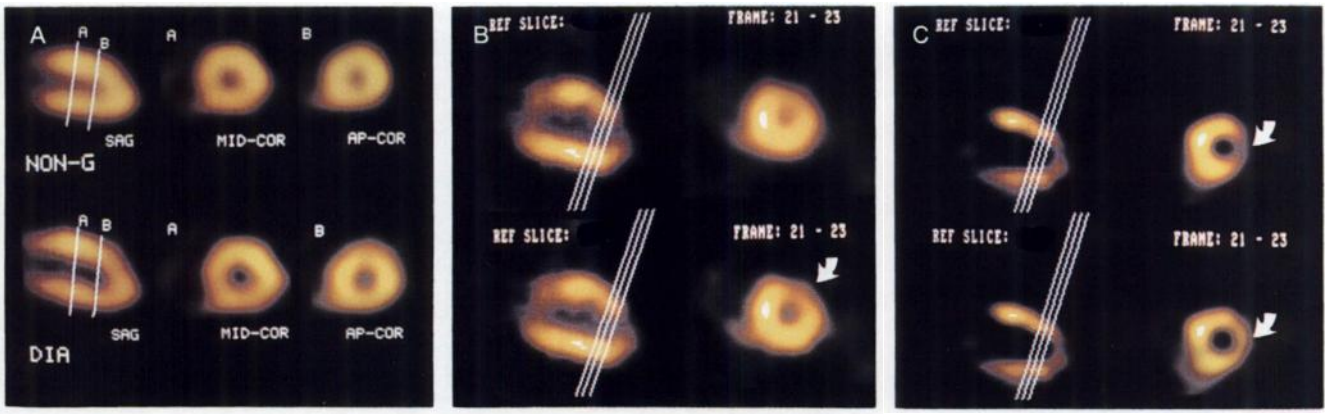

FIGURE 4. (A) Corresponding sagittal (mid-ventricular) images (left column) from nongated and gated (DIA) studies. Note extension of the LV cavity in apical direction in DIA study. Corresponding mid-ventricular and apical nongated (upper) and DIA (lower) coronal slices, each composed of three coronal slices at the level indicated by the lines. Note the larger LV cavity size in the DIA study. (B) Rest, nongated (upper) and DIA (lower), study in a patient with clinically verified infarct. Note low but nonsignificant antero-apical uptake in nongated study and significant (quantitatively confirmed) uptake defect in DIA study (arrow). (C) Stress study, nongated (upper) and DIA (lower) in a patient with a large perfusion abnormality in the lateral wall (arrows) with extension into the inferior wall and apex. Note the perfusion abnormality appears more severe in the nongated study (confirmed quantitatively).

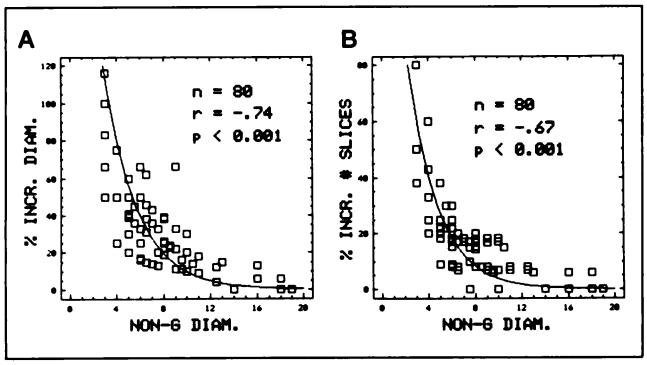

FIGURE 5. (A) The relationship between LV diameter in nongated studies and the increase (%) in LV diameter in diastolic images obtained from gated studies. (B) The relationship between LV diameter in nongated studies and % increase in the number of coronal slices in DIA studies.

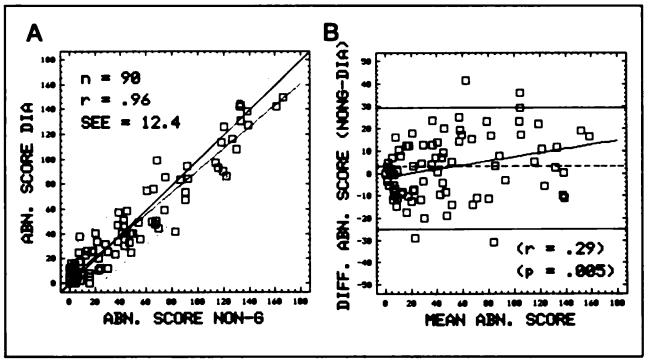

FIGURE 7. (A) Correlation between abnormality score (severity) in all rest and stress studies for the 45 patients with perfusion abnormalities. Line of identity is marked. Note the higher perfusion abnormality score in nongated studies for the majority of patients with large perfusion abnormalities. (B) Agreement between perfusion abnormality score with nongated and gated (DIA) imaging techniques and mean of nongated and DIA abnormality scores on the x-axis and difference between nongated and DIA abnormality scores on the y-axis. Note the systematic tendency or larger abnormality scores in nongated studies with large perfusion defects ($r = 0.29$, $p < 0.01$).

all had normal coronary angiography and no history of myocardial infarction.

In the remaining 45 patients, the perfusion abnormality score (severity) in the stress studies was higher in the nongated than in the DIA studies (56.6 ± 48.2 and 52.1 ± 43.5, respectively, $p < 0.05$), while no such differences were seen in the rest studies (38.0 ± 42.5 and 37.7 ± 40.1, respectively, $p > 0.05$, ns, Fig. 6). The correlation between perfusion abnormality scores in all nongated and DIA (rest and stress) studies was highly significant ($n = 90$, $r = 0.96$, $p < 0.001$, Fig. 7A). Also, when the nongated DIA abnormality scores were compared for the rest and stress studies separately, a high degree of correlation between assessed perfusion abnormality score emerged (both $r = 0.96$, $p < 0.001$). However, from these correlation graphs, it is apparent that even if the extent and degree of myocardial perfusion abnormalities correlate very well between the imaging techniques, differences in abnormality scores exist for patients with large perfusion defects. Analysis of agreement (*22*) between abnormality scores with the two imaging techniques further demonstrates such systematic differences (Fig. 7B). For small and medium-sized perfusion abnormalities, the agreement between the methods is very high. In patients with large perfusion abnormalities (score > approx 80 units), the abnormality score in nongated studies was higher than in DIA studies ($n = 21$, 119.2 ± 23.5 and 107.1 ± 29.5, respectively, $p = 0.0029$, Fig. 8). In patients with perfusion abnormality scores < 80 units, no significant difference between abnormality scores in nongated and DIA was found ($n = 69$, 25.4 ± 23.3 and 26.0 ± 27.8, respectively, $p = 0.72$, ns).

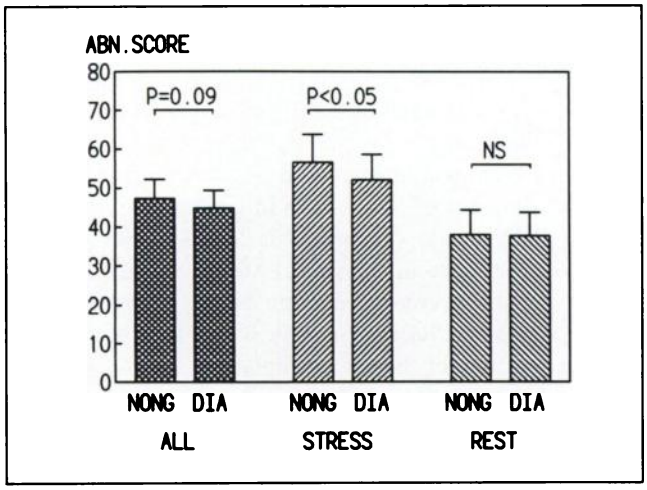

FIGURE 6. Abnormality score (severity) in all nongated and diastolic (DIA) studies (stress and rest) in subjects ($n = 45$) with perfusion abnormalities and abnormality scores in nongated and DIA studies for stress and rest studies separately.

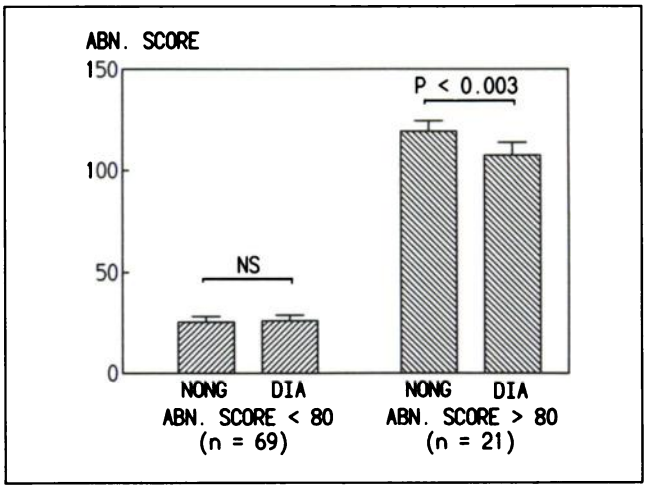

FIGURE 8. Abnormality score in nongated and DIA studies with small and moderate (score < 80 units) abnormalities and in studies with large perfusion abnormalities (score > 80 units).

For the individual patient, with reproducibility of abnormality score assessment taken into consideration (*18*), an abnormality score in DIA studies was larger than that in nongated studies in 8/90 (9%), equal in 60/90 (67%) and smaller in 22/90 (24%).

Reversibility

The difference in abnormality score between stress and rest studies (i.e., reversibility, expressed as reversibility score) in nongated and DIA studies correlated highly ($r = 0.89$, $p < 0.001$). Overall, the reversibility score with the two imaging techniques was not significantly different when all patients with perfusion abnormalities were seen as a group (22.0 ± 26.3 and 20.3 ± 21.8, respectively, $p = 0.36$, ns).

Concordance in Overall Outcome

Concordance of the quantified myocardial perfusion evaluations with the two imaging techniques in the 45 patients with abnormal perfusion was analyzed by classifying the overall results with each method (no perfusion abnormality, reversible abnormality, reverse reversibility or permanent abnormality). Identical overall outcome was found in 39/45 (87%) of the patients. In 6/45 (13%), discordant results emerged: one patient had a reversible abnormality detected in DIA studies only (abnormal coronary angiography), two patients had permanent defects in DIA studies only (both had clinical non-Q-wave infarcts) (Fig. 4C), two patients had permanent defects with nongated SPECT and reversible defects with DIA studies (both had abnormal coronary angiography with no clinical infarcts) and one patient had a permanent defect with nongated SPECT and reversibility in DIA studies (abnormal coronary angiography with no clinical infarct). Hence, no perfusion abnormality was detected in nongated studies that was not detected in DIA studies, while three had abnormalities in DIA only and two had reversible changes with DIA and permanent changes in nongated studies. In all six patients with discordant findings, the perfusion abnormalities were located in the apical third of the myocardium.

Dynamic Studies: Regional Function

The simultaneous display of the sagittal and coronal cine studies (Fig. 2) allowed visual assessment of regional wall motion in segments with normal or only slightly reduced radionuclide uptake. Minimal change along the epicardial contour during systole was noted. "Wall motion" was located on the endocardial contour which moved centrally during systole expressing the systolic wall thickening which courses the systolic decrease in LV volume. In segments with moderately decreased, low or no radionuclide uptake, visual estimation of regional wall motion was difficult or impossible. Further systematic visual analysis of regional function, expressed as wall motion, was therefore not performed.

The RV wall dynamics were clearly visualized in normals and near normal subjects. But again, when parts of the RV wall were missing (little or no tracer uptake), wall motion could not be graded.

DISCUSSION

In this series of consecutive patients, gated SPECT could be obtained in all but two patients at modest expense in camera/processing time. Access to an array processor made the technique clinically acceptable. In patients with arrythmia and RR times outside the predefined time interval, acquisition would stop until the next acceptable beat, which prolongs the study. In general, cases with irregular ventricular rhythm are not suited for gated SPECT.

RV wall motions were well visualized in the dynamic SPECT studies, an observation reported earlier in dynamic planar gated studies (*8*). In the DIA perfusion studies, the RV appeared more clearly demarcated and with higher contrast than in nongated studies. A logical explanation is that in nongated studies, the high RV motility observed in dynamic studies results in a blurred, low-contrast "smeared" image of the RV. In diastolic frames, the RV wall is captured in a phase with minimal movement leading to a sharp distinct image. The LV-to-BKG ratio in the nongated and DIA studies was not significantly different, which negates the possibility that a physiologically lower blood content in the lung during diastole explains the higher RV-to-BKG ratios in the DIA studies.

In the DIA studies, the LV cavity appeared larger and could be identified in more coronal slices in the apical direction than in the nongated studies (Fig. 5). Again, this can be explained as a logical effect of capturing the LV in diastole, thereby excluding the systolic obliteration of the LV cavity. Such increase in LV cavity size and extension improves qualitative and quantitative evaluation of myocardial perfusion, especially in the apical third of the myocardium. This was particularly evident in patients with small hearts and/or thick LV walls (situations where perfusion is notoriously difficult to evaluate in nongated SPECT). One could argue that the difference in LV cavity size between nongated and gated studies could be at least partially an effect of differences in the way subendocardial ischemia or injury are seen in the two types of studies. However, even in normals, LV size and the number of slices in the cavity were significantly higher in gated than in nongated studies, and the percentage increase in LV size was higher than in patients.

From the graph of the relationship between LV dimensions in nongated studies versus percentage increase in LV diameter and percentage increase in the number of coronal slices in the cavity (Fig. 5), one can extrapolate that in nongated studies for patients with a LV cavity size of less than 6–8 pixels (18–24 mm) the benefit of gated SPECT, i.e., better LV visualization, is the greatest

(>20%), while in patients with larger LV cavities (>8–10 pixels = 24–30 mm) little improvement is accomplished. The functional correlation to this reasoning is that in patients with large LV cavities, no real disturbing obliteration of the LV occurs in systole. Whereas in patients with small hearts or cavities, systolic obliteration of the cavity affects the images.

The LV appeared sharper and better demarcated in the DIA studies, but without higher contrast in relation to the BKG, probably because the LV wall has much smaller excursions than the RV during the cardiac cycle. Left ventricular volume decreases in systole mainly by an increase in LV wall thickness, which also observed with other dynamic tomographic modalities (two-dimensional echocardiography, gated MRI). Furthermore, details of LV perfusion abnormalities are apparently more realistically imaged in the DIA studies since the results in the DIA studies were in agreement with clinical data (verified infarction and results of coronary angiography) in the group of patients with subtle abnormalities and discordance between nongated and DIA studies. These findings are interpreted as the results of reduction of motion artifacts and controlling the partial volume effect by creation of diastolic studies from gated SPECT data. Interestingly, this improved ability to detect apical and small perfusion defects in gated studies was also noted in a recent study using intracoronary ^{201}Tl injection (high count studies) and gated planar imaging techniques (*23*). In the present study, the size of perfusion abnormalities varied markedly in the cine display, often decreasing in systole to the limit of being detectable. In high count studies using intracoronary thallium administration and gated planar techniques (*23*) and in a previous gated sestamibi SPECT study (*15*), it was noted that perfusion abnormalities appeared larger in diastolic frames than in systolic frames. The appearance of perfusion abnormalities in nongated studies therefore depends on the relative contribution of the systolic and diastolic phases to the nongated image, i.e., the appearance is affected by the heart rate during acquisition inasmuch as the diastolic fraction of the cardiac cycle varies with heart rate. This fact may be a contributing explanation to differences in perfusion abnormalities between gated and nongated studies in some patients, further advocating gated imaging to obtain realistic, diastolic images of perfusion.

A high degree of correlation between perfusion abnormality scores in the nongated and the DIA studies was found in the present investigation using a quantification method with documented high reproducibility (*17*). Thus, we have reason to believe that the close agreement between perfusion abnormality scores for small and moderate perfusion abnormalities reflects similar perfusion abnormality with nongated and DIA imaging techniques, while the systematic disagreement for large perfusion abnormalities indicates a real difference in perfusion abnormality score between the techniques, albeit small. The observed closer agreement between myocardial perfusion results with DIA imaging and clinical/coronary angiography results in detection of subtle abnormalities, and may be more important considering the diagnostic consequences. Detection of coronary disease (or not) and discrimination between established myocardial injury and ischemia may be clinically more relevant than differences in the severity of large perfusion defects.

Visual analysis of regional function expressed as wall motions was easily obtained in normal and in near normal segments, but could not be obtained in segments with moderate/severe perfusion defects (too little wall to evaluate). A similar limitation of gated dynamic perfusion images was recently reported in a study using gated planar techniques (*7*). The dynamic image display gave an overall clinically useful impression of LV size and function. The dynamic images are particularly valuable in patients with dilated left ventricles and only minor perfusion defects indicating dilated cardiomyopathy by demonstrating the striking discrepancy between regional perfusion and decreased function in such patients.

Assessment of regional LV function with the fractional shortening method (*8,9*) was not applied in this study since that method is based on definition of the endocardial borders at opposite LV walls when assessing the LV diameters in diastole and systole. Left ventricular diameters at locations with perfusion defects become very uncertain.

Regional function may still be obtainable from dynamic images by taking advantage of the partial volume effect. In experimental models (*10,11,24*), in planar gated ^{201}Tl studies (*10*) and gated ^{201}Tl SPECT studies (*11*), a connection between segmental systolic wall thickening (contractile function) and an increase in segmental counts from end-diastolic to end-systolic images (the partial volume effect) have been documented. An objective analysis of regional function in gated SPECT studies, applying the partial volume effect, is currently being analyzed in our institution.

In the present study, a temporal resolution of 8 frames per cardiac cycle was used. More frames per cycle is desirable and can be achieved at the expense of counting statistics and/or patient comfort by prolonging the acquisition. This has been achieved in gated planar imaging (*6–10*), though frame condensing was later used to obtain quality cines for evaluation of regional function. In gated SPECT studies where the inconvenience of a prolonged study with the arms over the head is considerable, end-diastolic and end-systolic images only (*11,13*), 8 frames/cycles (*15*), 16 frames/cycle (four patients) (*16*), or 18 frame/cycle (later condensed to 8 frames/cycle) (*25*) have been used. A temporal resolution of 8 frames/cycle can be seen as a limitation of the present study. On the other hand, the present gated SPECT method was designed to deliver end-diastolic images and dynamic studies for analysis of wall motion (and potentially systolic wall thicken-

ing). Assessment of thickening or thinning rates, requiring higher temporal resolution, was not attempted.

We conclude that the extra effort of gated SPECT is offset by clearer RV and LV imaging and improved image resolution. Gated SPECT is especially useful in patients with small hearts and/or LV cavities and in patients with subtle perfusion abnormalities. Large perfusion abnormalities are overestimated with nongated imaging. Regional function assessed as wall motion has limited usefulness.

REFERENCES

1. Hoffman EJ, Huang SC, Phelps ME. Quantitation in positron emission computed tomography: I. Effect of object size. *J Comput Assist Tomogr* 1979;5:391–400.
2. Aldersson PO, Wagner HN, Gomez-Moeiras JJ, et al. Simultaneous detection of myocardial perfusion and wall motion abnormalities by cinematic ^{201}Tl imaging. *Radiology* 1978;127:531–533.
3. Garty I, Kardontchik A. Study of ECG-gated thallium-201 myocardial scintigraphy; is imaging time a limiting factor? *Eur J Nucl Med* 1984;9: 173–176.
4. McKillop JH, Fawcett HD, Baumert JE, et al. ECG gating of thallium-201 myocardial images: effect on detection of ischemic heart disease. *J Nucl Med* 1981;22:219–225.
5. Hamilton GW, Narahara KA, Trobraugh GB, Ritchie JL, Williams DL. Thallium-201 myocardial imaging: characterization of the ECG-synchronized images. *J Nucl Med* 1978;19:1103–1110.
6. Hurwitz G, Schwab M, MacDonald AC, Driedger A. Quantitative analysis of myocardial ischaemia on end-diastolic thallium-201 perfusion images. *Eur J Nucl Med* 1990;17:257–263.
7. Verzijlbergen JF, Suttorp MJ, Ascoop CAPL, et al. Combined assessment of technetium-99m sestamibi planar myocardial perfusion images at rest and during exercise with rest/exercise left ventricular wall motion studies evaluated from gated myocardial perfusion studies. *Am Heart J* 1992;123:59–68.
8. Maisey MN, Mistry R, Sowton E. Planar imaging techniques used with technetium-99m sestamibi to evaluate chronic myocardial ischemia. *Am J Cardiol* 1990;66:47E–54E.
9. Najm YC, Timmis AD, Maisey MN, et al. The evaluation of ventricular function using gated myocardial imaging with ^{99m}Tc sestamibi. *Eur Heart J* 1989;10:142–148.
10. Marcassa C, Marzullo P, Parodi O, Sambuceti G, L'Abbate A. A new method for noninvasive quantitation of segmental myocardial wall thickening using technetium-99m 2-methoxy-isobutyl-isonitrile scintigraphy — results in normals subjects. *J Nucl Med* 1990;31:173–177.
11. Mochizuki T, Murase K, Fujiwara Y, Tanada S, Hamamoto K, Tauxe WN. Assessment of systolic thickening with thallium-201 ECG-gated single photon emission computed tomography: a parameter for local left ventricular function. *J Nucl Med* 1991;32:1496–1500.
12. Kahn JK, Henderson EB, Akers MS, et al. Gated or ungated tomographic perfusion imaging with technetium-99m RP-30A: comparison with ^{201}Tl tomography in coronary artery disease [Abstract]. *J Am Coll Cardiol* 1988;11:31.
13. Larock MP, Cantineau R, Legrand V, Kulbertus H, Rigo P. ^{99m}Tc-MIBI (RP-30) to define the extent of myocardial ischemia and evaluate ventricular function. *Eur J Nucl Med* 1990;16:223–230.
14. Sochor H, Huber K, Probst P, et al. Assessment of myocardial perfusion and wall motion by the new perfusion agent ^{99m}Tc-MIBI and SPECT [Abstract]. *Eur Heart J* 1988;9:I-364.
15. Grucker D, Florentz P, Oswald T, Chambron J. Myocardial gated tomoscintigraphy with ^{99m}Tc-methoxy-isobutyl-isonitrile (MIBI): regional and temporal activity curve analysis. *Nucl Med Commun* 1989;10:723–732.
16. Faber TL, Akers M, Peshock R, Corbett JR. Three-dimensional motion and perfusion quantification in gated single photon emission computed tomograms. *J Nucl Med* 1991;32:2311–2317.
17. Mannting F, Morgan MG, Maripuu E. Quantification of myocardial perfusion abnormalities in SPECT studies using ^{201}Tl or sestamibi protocols. *Int J Card Imaging* 1992:in press.
18. Taillifer R, Laflamme L, Dupras G, et al. Myocardial perfusion imaging with ^{99m}Tc-methoxy-isobutyl-isonitrile (MIBI): comparison of short and long time intervals between rest and stress injections. *Eur J Nucl Med* 1988;13:515–522.
19. King M, Doherty PW, Schwinger RB. Fast count-dependent digital filtering of nuclear medicine images: concise communication. *J Nucl Med* 1983;24:1039–1045.
20. Larsson SA. Gamma camera emission tomography. *Acta Radiologica* 1980;(suppl):363.
21. Quan-Sheng Li, Solot G, Frank TL, et al. Myocardial redistribution of technetium-99m-methoxyisobutul isonitrile (sestamibi). *J Nucl Med* 1990; 31:1069–1076.
22. Bland JM, Altman DG. Statistical methods for assessing agreement between two methods of clinical measurement. *Lancet* 1986;1:307–310.
23. Siegel ME, Chen DCP, Lee K, et al. Gated intracoronary thallium-201 scintigraphy: feasibility and potential clinical advantages. *Angiology* 1989;40:513–520.
24. Galt JR, Garcia EV, Robbins WL. Effects of myocardial wall thickness of SPECT quantification. *IEEE Trans Med Imaging* 1990;9:144–150.
25. Sochor H. Technetium-99m sestamibi in chronic coronary artery disease: the European experience. *Am J Cardiol* 1990;66:91E–96E.